Pinbone Detection of Japanese Shime-Saba by Near-Infrared Imaging

Hisayoshi Ito Oky Dicky Ardiansyah Prima Takehiro Sasaki
Graduate School of Software and Information Science
Iwate Prefectural University
152-52, Sugo, Takizawa, Iwate, Japan
e-mail: {hito, prima}@iwate-pu.ac.jp, g231t201@s.iwate-pu.ac.jp

***Abstract*—There is a growing demand for new analytical techniques to manage the presence of fish bones more effectively. The detection of fish bones involves human inspection using touch and vision, which can lead to misjudgment. Many studies utilize X-ray machine vision approaches to effectively detect fish bones in quality control processes. However, this approach requires complex devices and carries the risk of radiation exposure. In this study, we attempted to detect the pinbone tip locations of shime-saba by using Near-Infrared (NIR) machine vision to highlight those features and quantify them based on image geometry and neural networks. The vinegar added to the shime-saba softens most of the bones, but the pinbones remain tough and need to be removed. Our approach is as follows. At first, the fish fillet is photographed with NIR transmitted through the fish fillet. The resulting image is correlated with the Gaussian template image. Quadratic surface equations are performed on the automatically defined Region of Interest (ROI) for this image and the convex-up shapes are selected as candidates for the pinbone tips. Rectangular areas (sub-images) of ten candidates are extracted and a Convolutional Neural Network (CNN) is constructed using these sub-images to determine the presence of pinbones. In the experiment, 95 samples of shime-saba fillets were captured in NIR, and 950 sub-images (225 contained pinbones) were extracted to train the CNN model. As a result, the CNN model was able to determine the bone with 84.9% accuracy.**

Keywords-fishbone; near-infrared imaging; bone detection; image geometry; convolutional neural network.

I. INTRODUCTION

There is an increasing need for improved quality inspection and visibility into the food supply chain to ensure food safety, quality, and traceability. This paper is an extension of our previous work on an automated method for detecting pinbones of shime-saba [1], a traditional Japanese fish dish.

Sushi and sashimi are among the most famous Japanese dishes. Such fishery products have had a significant influence on the Japanese diet for centuries. In addition to fresh fish, there have also been many seafood products developed for long-term preservation. Traditional Japanese seafood preparations include shime-saba (mackerel marinated in sugar, salt, and rice vinegar) and dried or salted fish. Hachinohe City in Aomori Prefecture is home to shime-saba, the first city in Japan to begin producing this fish dish in 1968. Although the number of mackerel landings is on the decline, production of shime-saba is on the rise. However, this growth is difficult to maintain in Japan due to a chronic shortage of human resources, requiring the automation of production processes.

To increase efficiency in the food industry, methods are being developed to automate production processes [2]. Robotics may play an important role as a solution. However, compared to other industries, the food industry has been slow to adopt robotics. The use of robots is expected to bring many tangible, intangible, social, and economic benefits [3]. The risks associated with sanitation and safety, as well as high labor and social costs, will promote the adoption of robots in the food industry.

The fisheries industry has traditionally been a labor-intensive sector and required skilled staff to process the fish into consumable products. Processing included filleting, trimming, peeling, visual inspection for parasites, and quality control [4]. Another process of trimming is the removal of pinbones. The pinbone can be removed by hand because its attachment tends to weaken after rigor.

The Japanese food industry is actively introducing robots to the market. However, it is difficult for small and medium-sized companies to introduce robots for processing typical fish on their own. In addition, the processing of shime-saba requires human handling to remove the pinbones that remain on the fish fillet. The vinegar added to the shime-saba softens most of the bones, but the pinbone remains tough and needs to be removed by hand. Since pinbones are difficult to see, this job is physically demanding because it involves touching the fish fillet, sensing the presence of pinbones, and then removing those bones with tweezers. It also requires more workers to ensure production capacity. The manual removal of the remaining pinbones from the shime-saba can be seen in Figure 1. These bones are in the middle of the cross-section of the filleted fish body. Since the cross-sectional height of shime-saba is only about 1-3 cm, deboning automatically from that position is considered challenging.

The purpose of this study is to improve on our previously developed image sensing system for detecting the pinbone tips of shime-saba to assist in deboning robots [1]. The new system automatically detects the tip of the bone by analyzing features from Near-Infrared (NIR) images of the fillet of shime-saba. Pinbone detection is performed in two stages: selection of local convex-up regions based on mathematical quadratic surfaces and determination of the regions containing pinbone tips based on Convolution Neural Network (CNN). Finally, the implementation of this system is described and further improvements in detection accuracy are discussed.

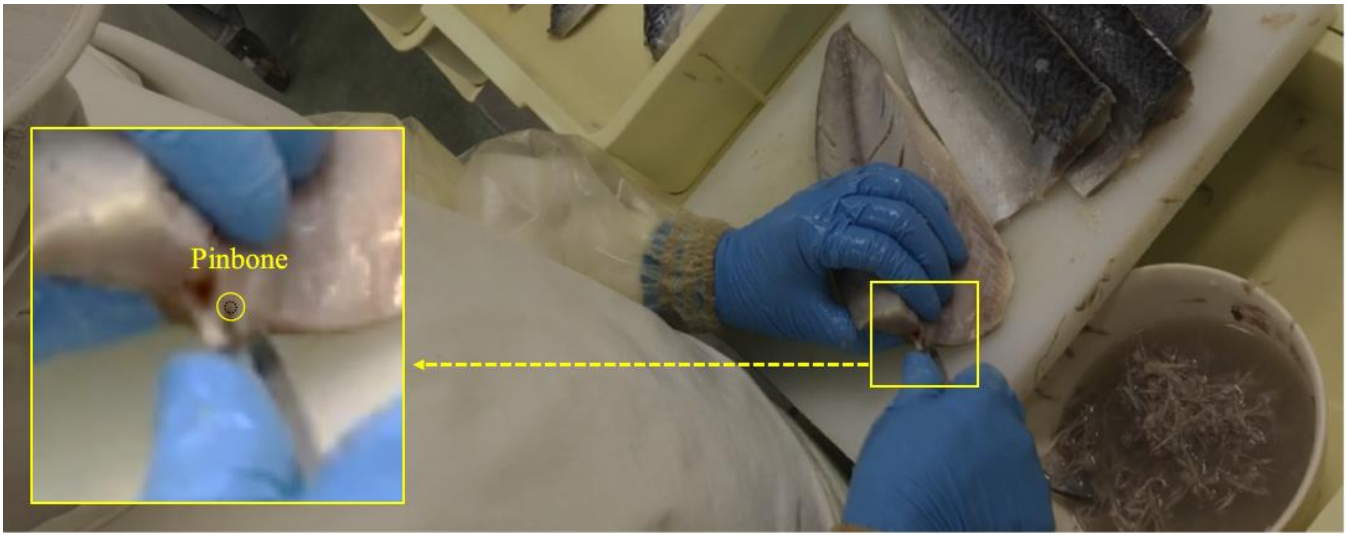

Figure 1. Manual removal of the pinbones remaining in the middle of the cross-section of the fillet.

The rest of this paper is organized as follows. Section II describes related works on fish bone detection using image sensing techniques. Section III describes our proposed methods for detecting pinbone tips from NIR transmitted images. Section IV describes our experiments and summarizes the results. Section V provides a discussion of improving the determination of areas that limit the analysis area for efficient pinbone tip detection. Finally, section VI concludes our work.

II. Related Works

Traditionally, removing bones from fish fillets has involved the use of tweezers or needle nose pliers. Currently, hand-held pinbone removers are available and allow for easy deboning manually. To remove bones using these tools, the tip of the bone must first be located. Hence, finding the tip of the bone is an important step in automating the deboning process.

Various applications using image sensing inspection have been developed to ensure food safety. For detecting fish bones, image sensing techniques such as X-ray, Ultraviolet (UV), and NIR spectroscopy have been proposed. Mery et al. developed an X-ray machine vision approach to detect bones in fish fillets [5]. Their device is a digital radiography system consisting of an X-ray source and a flat panel detector. Filter banks including Discrete Fourier Transform (DFT), Discrete Cosine Transform (DCT), and Gabor were used to extract features from the resulting X-ray images. The results showed that by photographing the fish bones, which are arranged in strips and range from 14 mm to 47 mm in length, these bones can be detected with a high accuracy. Andriiashen et al. introduce a processing method for unsupervised foreign body detection based on dual-energy X-ray absorption measurements. Their method results in improved X-ray-based bone detection [6]. Wang et al. investigated the fluorescent properties of cod bone under UV irradiation and found that the optimum wavelengths of excitation and emission were 320 nm and 515 nm. They were the first to develop UV fluorescence-assisted candling for detecting fish bones, but the detection accuracy was lower than that of X-ray-based techniques [7]. Wei et al. used infrared spectroscopy to identify fish bone contents in surimi. The absorption peak in the infrared spectrum at around 9,890 nm wavelength was observed from fish bones [8]. Song et al. proposed a fish bone detection based on Raman hyperspectral imaging technique to improve detection rate and achieve automatic detection [9]. This technique was found to effectively detect fish bones down to a depth of 2.5 mm.

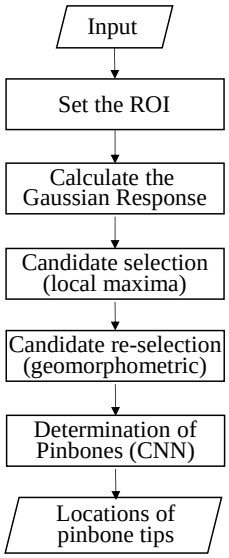

Figure 2. Detection of pinbone tips for this study.

The above optical sensing at various wavelengths has been used to bring up the feature values of fish bones to locate the position of the bones in the body of the fish. However, putting

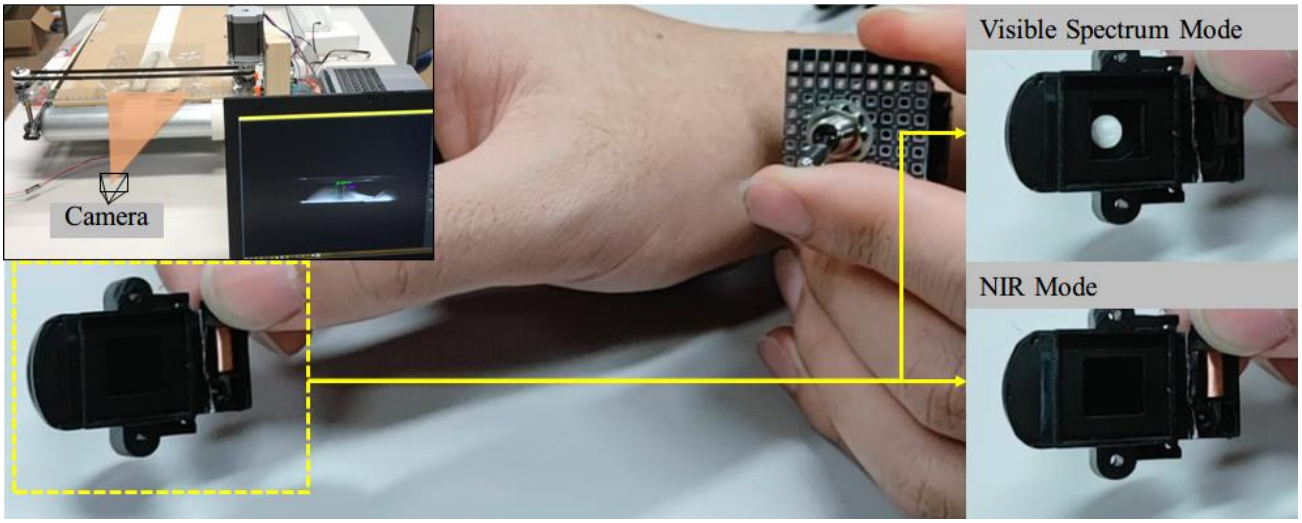

Figure 3. The device for NIR imaging in this study.

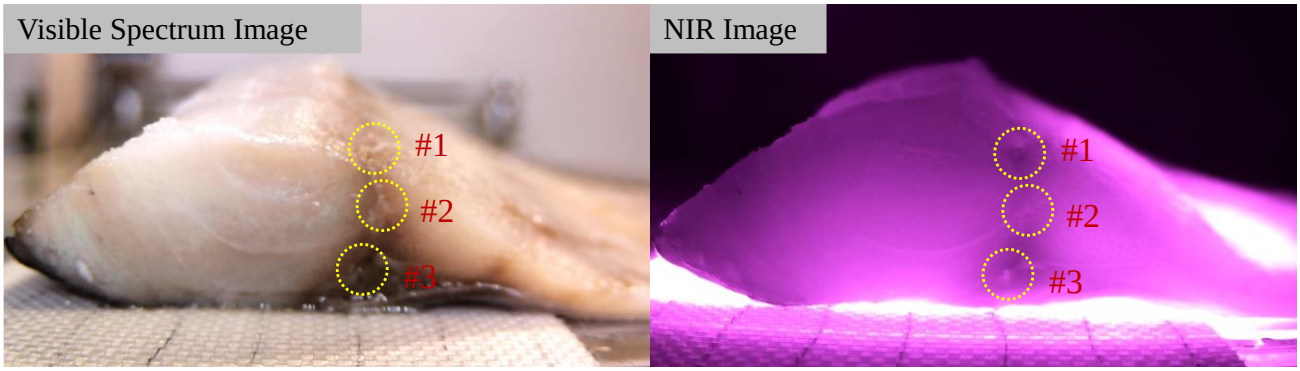

Figure 4. Three bones in the shime-saba.

these technologies to practical use in food processing facilities is problematic due to their high cost. Furthermore, while it can detect bones of a certain length, it is not capable of detecting objects where only the tip of the bone can be seen. In contrast, the NIR-based approach proposed by Prima et al. was able to highlight the presence of pinbone tips by image correlation between NIR and Gaussian template images [1].

III. METHODS

In this study, we focus on the broad application of NIR to food analysis, based on various sample presentation techniques [10]. In addition to reflection, NIR absorbed and transmitted from the sample may be used to detect the presence or absence of pinbones in the fish fillet. Here, we attempt to detect the tips of pinbones by photographing the NIR transmitted through the fish fillet.

Figure 2 shows an overview of our pinbone tip detection. After capturing a fillet of shime-saba, the region of interest (ROI) where the pinbone is likely to be located is estimated. Since the pinbone of the shime-saba remains in the center of the cross-section of the fillet, assigning this region as a ROI reduces the processing cost of its detection. This ROI estimation involves locating the backbone of the fillet. The NIR image within the ROI is then correlated with a predefined Gaussian template image to produce a Gaussian response image. Regions with maxima in the response image are selected as candidates for those consisting of the pinbone tip. Geomorphometric features are calculated for these regions, and regions with convex-up features are selected as final candidates. Finally, a CNN model is built based on these regions, and the presence or absence of pinbone tips in each region is determined.

A. Image Acquisition

The device for NIR imaging in this study is shown in Figure 3. The camera can capture images in the wavelength range from visible spectrum to NIR spectrum. To obtain images in each spectrum, a dynamic infrared filter is attached to the camera lens. Arduino hardware and software were used to switch the filters. By switching these filters electronically, both visible and NIR images of the fillets can be taken at the same position and orientation. For the NIR source, eight 840 nm NIR LEDs were used. The LEDs were arrayed beneath the conveyor belt. The camera resolution is 1280x720 pixels.

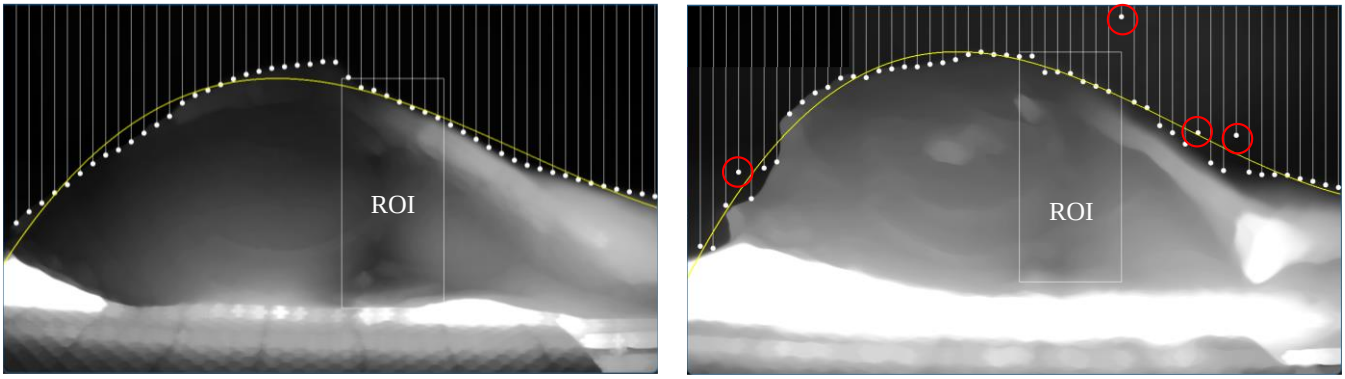

(a) Proper detection of the upper boundary points of the fillet (b) Incorrect detection of a part of the upper boundary points of the fillet

Figure 5. Determining the ROIs.

As shown in Figure 4, there are a maximum of three pinbones to be deboned. The presence of these bones is not clear in the visible spectrum image, so deboning staff must touch the fillet with a tweezer to check for their presence. In contrast, the NIR image reveals features at the tip of the pinbone. The tips of the pinbone appear to be locally bright and to have a convex-up surface in the NIR image.

B. Determining the ROI

In the cross-section of the shime-saba fillets, the pinbone tips to be detected are known to be located on the backbone of the fillet relative to the stomach. Since the most raised portion of the fillet is where the backbone was originally located, identifying this area will lead to the identification of the ROI. To automatically identify this location, a vertical edge detection filter (Sobel) is applied to the near-infrared image of the fillet, and the resulting edge image is scanned from top to bottom for all columns to find points where pixels exceed the threshold value. A cubic polynomial

$$f(x) = Ax^3 + Bx^2 + Cx + D. \quad (1)$$

is applied to these points to estimate the shape of the upper part of the fillet. Here, x, y are the coordinates of the points obtained from scanning. A to D are the coefficients for the cubic polynomial calculated by the least squares method. If the location of the maximum of the curve of the cubic polynomial is on the left side of the fillet image, the stomach is considered to be on the right side, and vice versa.

The resulting ROIs are as shown in Figure 5. Despite the presence of some incorrectly detected upper boundary points of the fillet (red circles) as shown in Figure 5(b), the cubic curve approximately traces the fillet's boundary (yellow lines).

C. Gaussian Response

To enhance the features of the bone tips in the NIR image, this image is correlated with a Gaussian template image. The formula of a Gaussian function in two dimension is

$$f(x,y) = \frac{1}{\sqrt{2\pi\sigma^2}} e^{-\frac{x^2+y^2}{2\sigma^2}}. \quad (2)$$

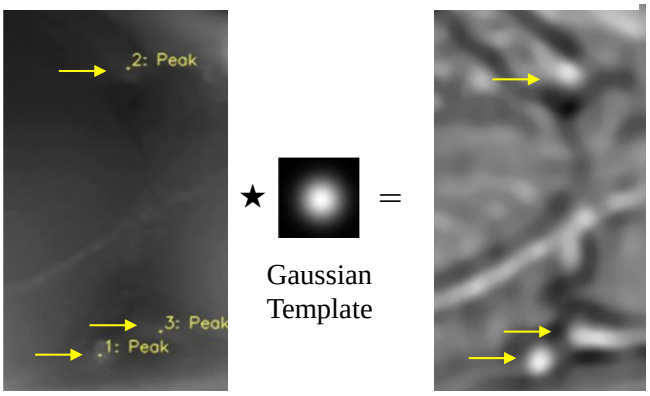

Figure 6. The response image obtained by pre-processing.

where x, y is the distance from the origin in the horizontal and in the vertical axes, respectively. σ is the standard deviation of the Gaussian distribution. As shown in Figure 6, the response image obtained shows that the center of the image is bright in the region at the tip of the bone. If the brightness of this image is taken as an elevation, the region at the tip of the bone can be thought of as a convex-up surface. The extent of the convex-up structure can be adjusted by changing the size of the Gaussian template image. For this study, the size was empirically determined to be 45 x 45 pixels with σ = 5 pixels.

D. Rectangular Areas of Pinbone Tip Candidates

The rectangular area centered on the brightest spot of the response image is selected as the candidate area (sub-image) for the pinbone tip. This spot is extracted by calculating the local maxima of the response image. A threshold is set as the distance between a point of maxima and the next point of maxima. Here, the size of the area is set to 45 x 45 pixels and the minimum distance between the points of maxima is set to 20 pixels.

E. Geomorphometric Features of Pinbone Tip Candidates

We developed a morphometric characterization algorithm to determine geomorphometric features (e.g., peaks, pits, ravines, or ridges) from previously described rectangular

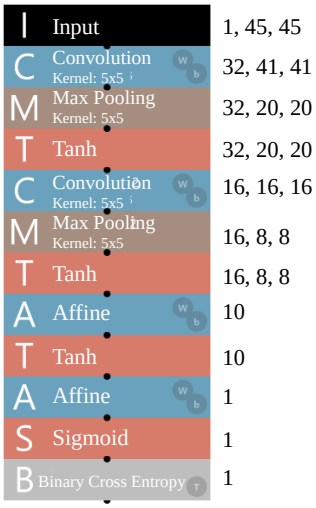

Figure 7. The CNN used for this study.

areas of the pinbone tip candidates. The quadratic surface is fitted to the image within a moving local analysis window using least-squares [11], with the general equation being

$$z = f(x, y) = Ax^2 + Bxy + Cy^2 + Dx + Ey + F. \quad (3)$$

where (x, y) is the location's coordinate, z is the pixel value calculated by the quadratic function, and A to F are the coefficients of the quadratic function calculated by the least squares method. By analyzing the second-order coefficients A to C, the shape of the quadratic surface can be characterized as follows.

$$\text{Elliptic paraboloid:} \quad B^2 - 4AC < 0 \quad (4)$$

$$\text{Hyperbolic paraboloid:} \quad B^2 - 4AC > 0 \quad (5)$$

$$\text{Parabolic paraboloid:} \quad B^2 - 4AC = 0 \quad (6)$$

Here, if A=B=C=0 then the quadratic is a plane. Equation (2) divides the quadratic surface into convex-up and concave-up. If the center of the convex-up surface is within the analysis window, this surface can be determined as the peak. As shown in Figure 4, the pixel of the pinbone tip is brighter than its neighbors, which means that this pixel represents the convex-up (peak). Hence, this property can be used to determine the location of the pinbone tips from the response image.

F. Determination of Pinbone Tip Using CNN

Regions with convex-up features do not necessarily contain pin bones. We introduce a CNN that determines the presence of pin bones among those regions. Our CNN architecture is shown in Figure 7. This network was built using the Neural Network Console [12], an engineer-oriented deep learning framework developed by Sony Group Inc. The input to the CNN is a 45x45 rectangular area of the pinbone candidate. Signals are passed through a two-stage network consisting of convolution, maximum pooling, and tanh activation function. The first stage produces 32 maps and the second stage 16 maps. The results are fully concatenated and the presence or absence of pinbone is determined by binary cross entropy. The Mean Squared Error (MSE) is used as the loss function for the network optimization process.

To summarize, the process to build a dataset of pinbones in shime-saba fillets is as shown in Figure 8. The first process is to find the boundary points (white circles) between the top point of the fillet and the background based on the edge intensities calculated from the input NIR image. From these points, a cubic curve (yellow line) is approximated to find the highest point of the fillet. The ROI is then placed at the same height as the top point in the stomach direction. Ten rectangular areas of candidate pinbones are automatically extracted. These areas are assumed to have both local maxima

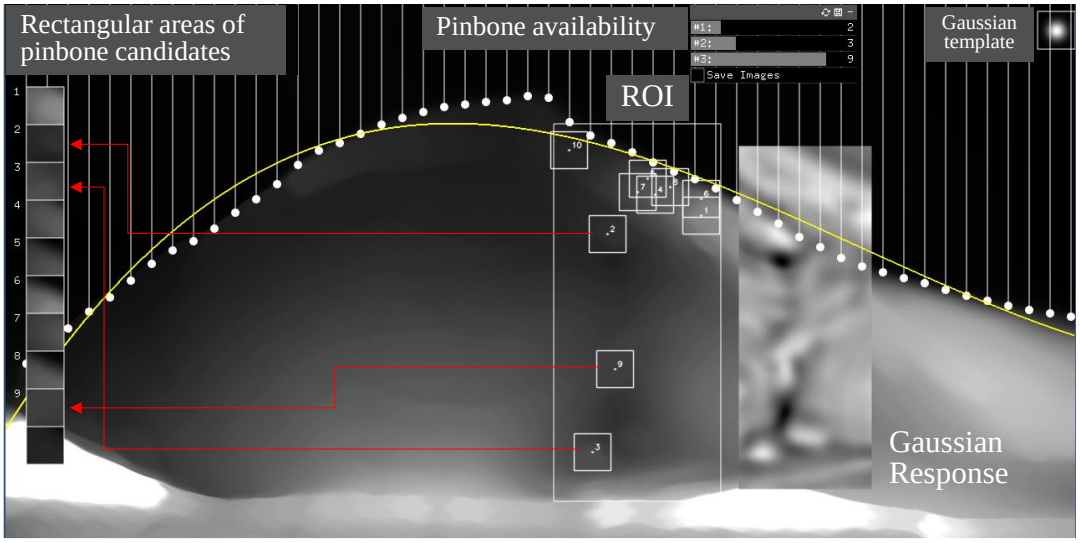

Figure 8. A GUI created to build a dataset of pinbones in the shime-saba.

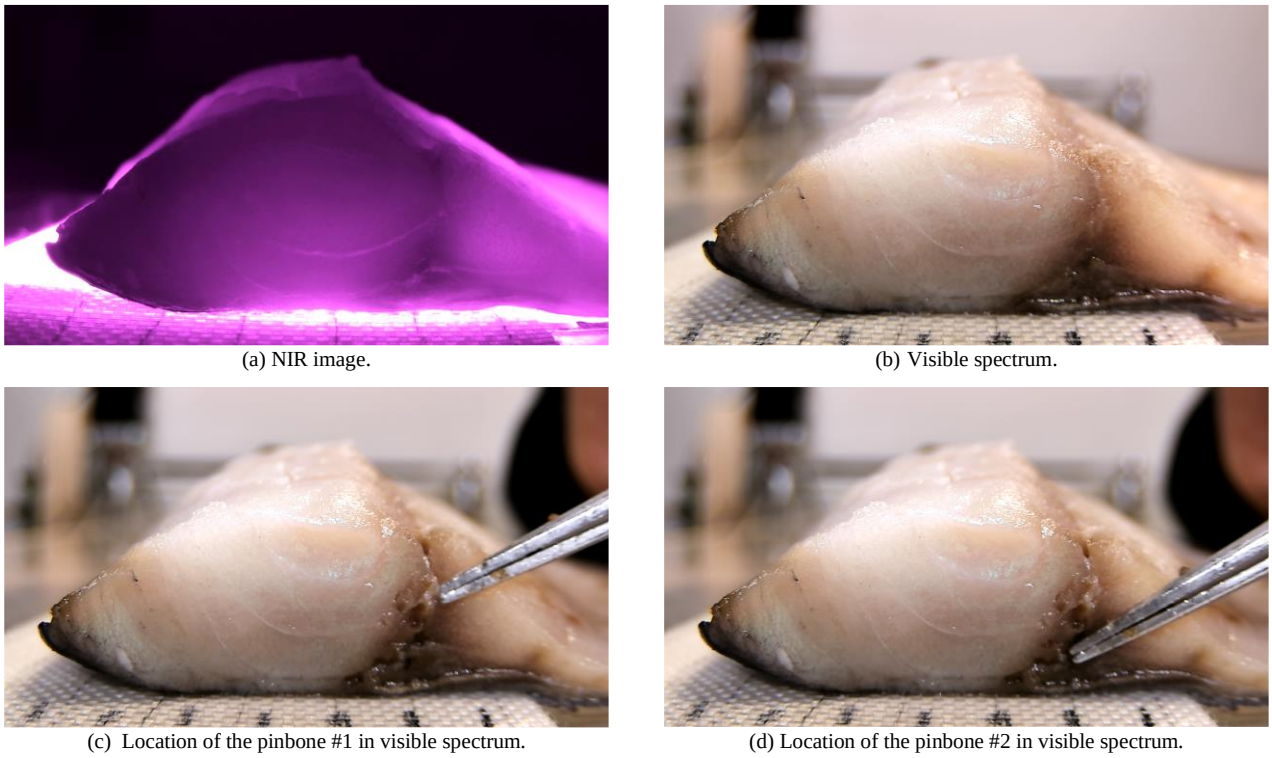

(a) NIR image. (b) Visible spectrum.

(c) Location of the pinbone #1 in visible spectrum. (d) Location of the pinbone #2 in visible spectrum.

Figure 9. An example of images of a fillet taken for this experiment.

and convex-up features, which are confirmed by quadratic equations. Finally, using the GUI (slider), the presence/absence label of the pinbone tips are given to these rectangles, and they are constructed into a dataset learnable by the CNN. Here, samples with pinbone tips are classified as positive and those without pinbone tips as negative in the dataset. OpenCV (opencv.org), an open-source computer vision software library, is used for this calculation.

IV. Experiments and Results

For this experiment, 95 shime-saba fillets were used. These fillets were taken from the shime-saba production process before they were packaged. Fillets with less cracks were chosen for the experiment to avoid extra NIR light influence from the cracks.

A. Image Acquisition

The fillets are photographed in the order of NIR and visible spectrum, and then the pinbones are located with tweezers and the scene is photographed as well. For each fillet, the images are taken as shown in Figure 9, facilitating easy generation of the positive images in the dataset that contains pinbones. From the 95 fillets of shime-saba photographed in this study, 250 locations of pinbones could be identified manually with tweezers. This means that there are around two to three pinbones in each fillet.

B. Region of Interest (ROI)

The size of the ROIs was fixed at 200 x 400 pixels and located at 175 pixels away from the top of the approximated curve of the fillet. Figure 10 shows the results of some typical ROIs. The blue dotted lines indicate the potential location of pin bones. The ROIs were determined for 95 fillets of shime-saba, with 78 ROIs covering the area where the pinbone tips are present. In addition, 14 ROIs partially covered the area where the pinbone tips are present. Only three ROIs did not correctly cover the pinbone tips. As the side of the fillet floats off the conveyor belt, the ROI falls off the pinbone positions. In this study, ROIs that did not properly cover the pinbone were manually transformed to cover the area where the pinbone was present.

C. Ten Candidates for Pinbone Tips

From each fillet, ten rectangular areas where pinbones potentially exist were selected in order of their convexity calculated by Equation (2). These rectangular areas were labeled for the presence or absence of pinbone tips by comparing them to locations indicated by the tweezers in the visible spectrum image of the fillet as shown in Figure 9. The top ten candidate rectangular areas were obtained from 95 fillets, for a total of 950 rectangular areas. Of those, 225 pinbones could be identified, but the remaining 25 could not. Extracting the top ten pinbone tip candidates for each fillet means that 90% of the pinbone tips can be located. However, since only a maximum of three pinbone tips are present in the cross-section of each fillet, the ten candidates must be further narrowed down. Finally, a binary classification dataset was constructed with 225 rectangular areas with confirmed pinbone tips as positive and the remaining 725 rectangular areas as negative samples.

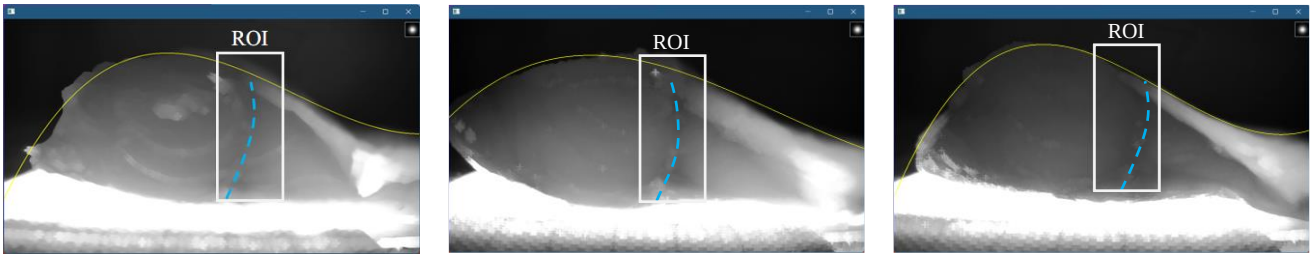

(a) ROIs covering the area where the pinbone tips are present.

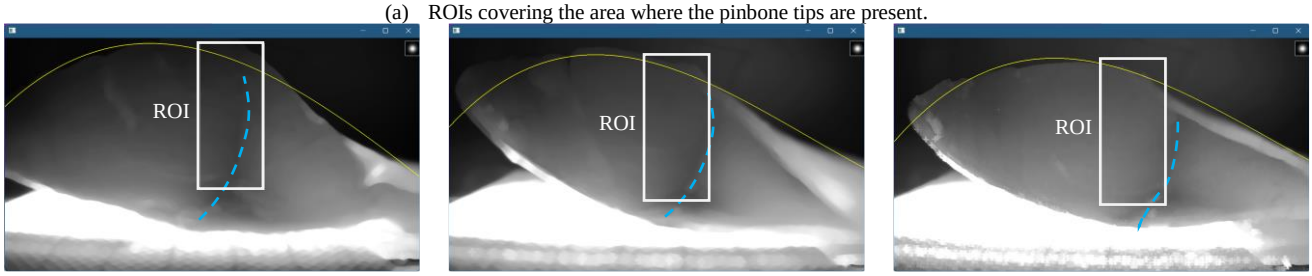

(b) ROIs partially covering the area where the pinbone tips are present.

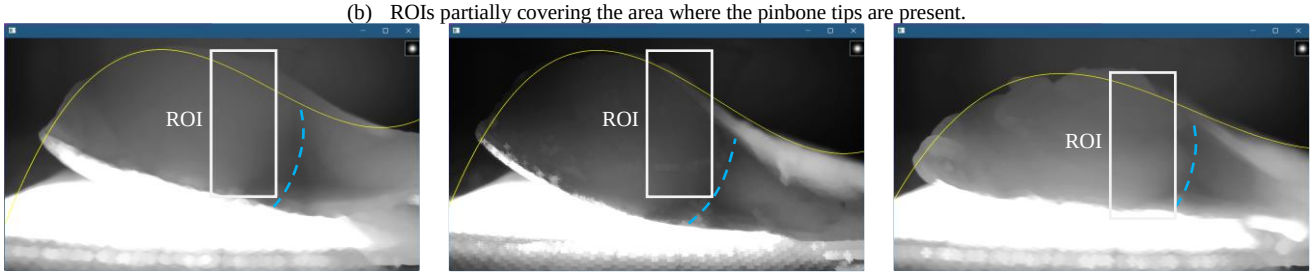

(c) ROIs does not cover the area where the pinbone tips are present.

Figure 10. ROIs automatically identified by this study.

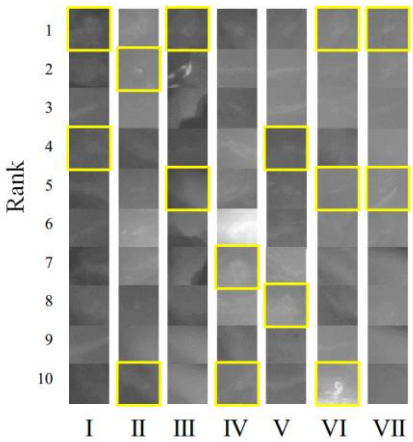

Figure 11. Rectangular areas from seven fillets (I~VII)

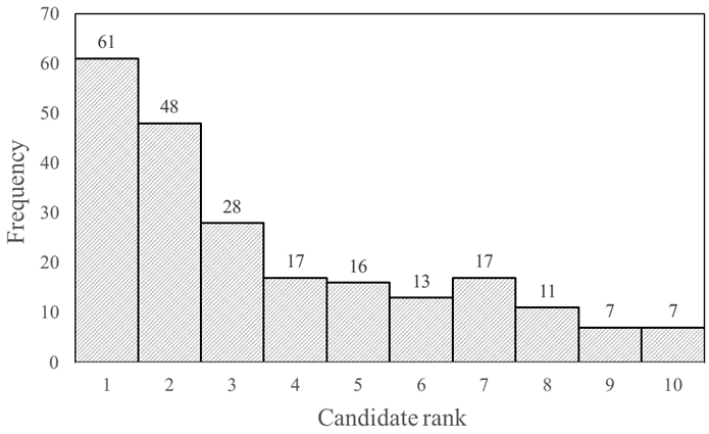

Figure 12. The relationship between rank and pinbones.

Figure 11 shows ten candidate rectangular areas extracted from seven fillets (I - VII). Yellow boxes indicate the presence of pinbone tips within the areas. Overall, the relationship between the rank of 10 candidate areas and the number of pinbones present is shown in Figure 12. Here, a higher rank can be interpreted as the presence of more pinbone tips. In other words, the presence of pinbone tips suggests that they can be found in the NIR image of the fillet where the convexity is high.

D. Determination of Pinbone Tip Using CNN

Using the previously described binary classification dataset, we trained the CNN as shown in Figure 7. About 80% (760 rectangular areas) were randomly selected for training and 20% (190 rectangular areas) for validation. Here, the batch size was set to 32, the epoch to 100, and Adam was used as the optimizer. The cost function, training error, and validation error of the CNN measured after each epoch are

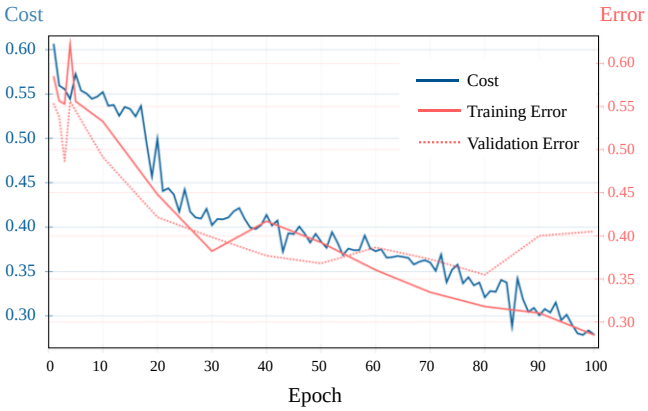

Figure 13. Learning curve of the CNN in this study.

TABLE I. CONFUSION MATRIX

		Predicted values	
		Negative	**Positive**
Real values	**Negative**	138	14
	Positive	15	25

Accuracy	0.849	**Recall**	0.625
Precision	0.641	**F-Measures**	0.633

shown in Figure 13. Up to the 80th epoch, the validation error decreases but begins to increase again. Therefore, at the 80th epoch, the model weights were outputted since the loss is low and stable. Table I shows the confusion matrix of the learned CNN model. Accuracy was good at 84.9%, but precision, recall, and F-Measures were relatively low at just over 60%. The reason can be attributed to the small sample size of the dataset and to positive samples being only about 30% of the total number of negative samples. The results of this study, however, are encouraging as a first attempt in this effort, and we believe that the results can be improved further by increasing samples in the dataset and by improving the method of determining the ROI and the design of the CNN.

V. DISCUSSION

The ROI of this study, which limits the analysis area for efficient pinbone tip detection, is expected to not only reduce the computational cost but also reduce misdetections. However, identifying the boundary points of the fillets by edge intensity and approximating those points with a cubic curve is susceptible to influence by noise. In addition, when multiple fillets are side-by-side, calculation of the cubic curves according to each fillet becomes more complicated.

For future development, we experimented with the use of CNN-based semantic segmentation to estimate the boundaries of fillets as shown in Figure 14. There are two main parts: a contraction pass consisting of a convolution layer unit and an expansion pass consisting of a deconvolution layer unit. Each convolution is followed by batch normalization and Rectified Linear Unit (ReLU). Input data consisted of NIR images of 95 fillets of shime-saba fillet used in our experiment and manually annotated fillet shapes.

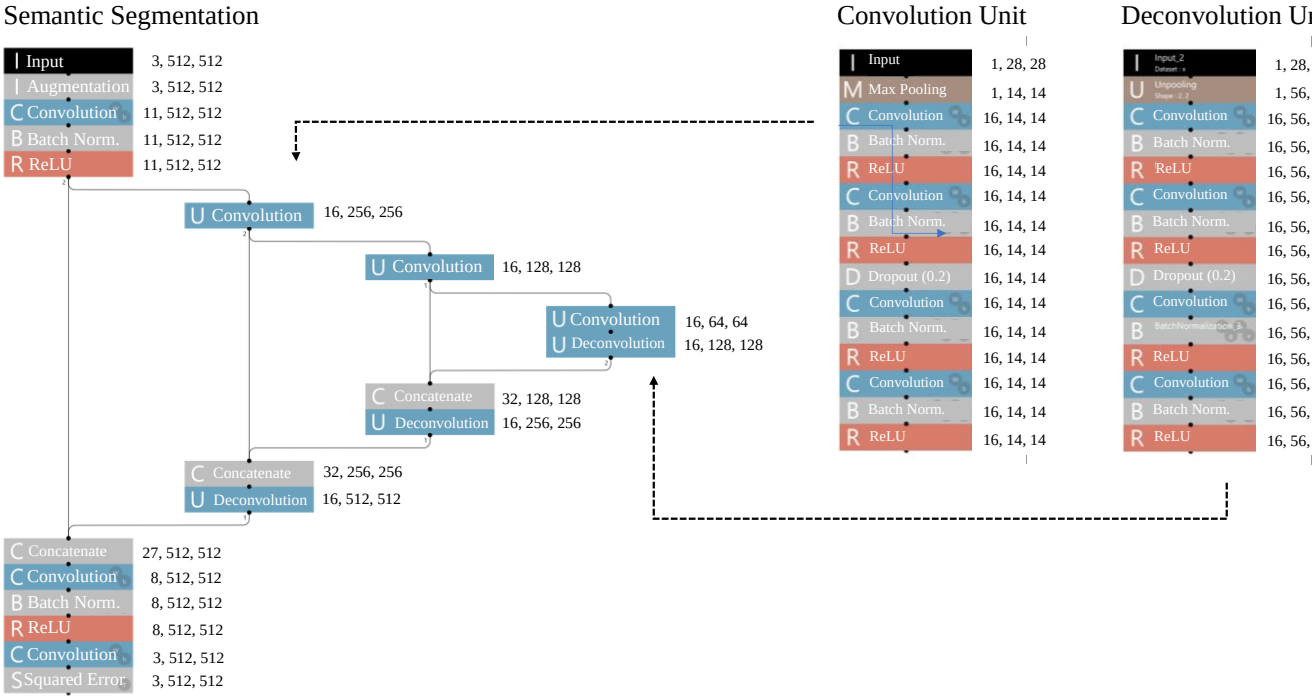

Figure 14. Neural network of the semantic segmentation for this study

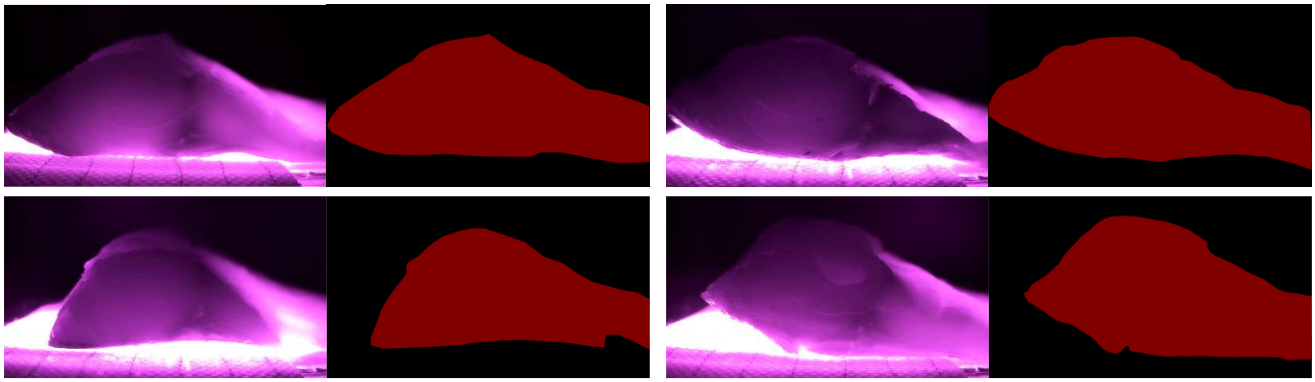

(a) Manually annotated shime-saba fillets.

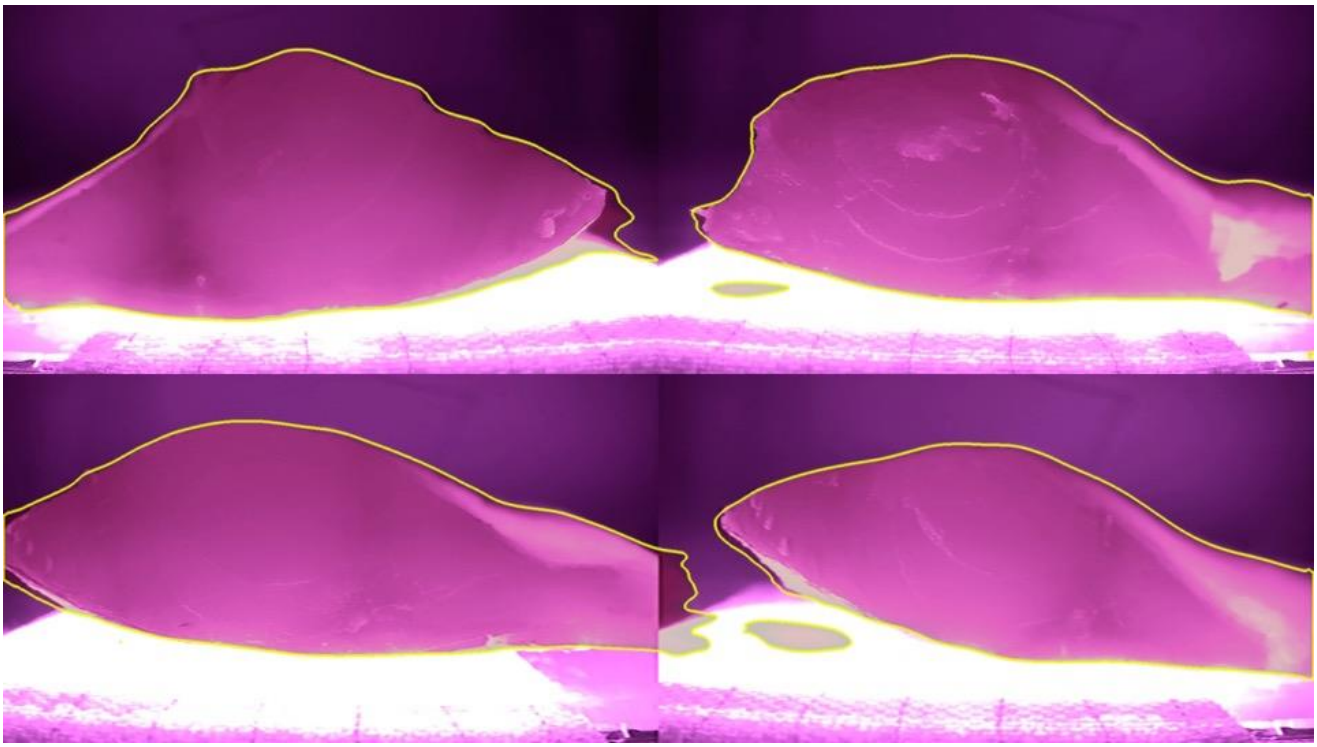

(b) Fillet shapes detected using the CNN-based semantic segmentation

Figure 15. Manually annotated shime-saba fillets and fillet shapes detected using the CNN-based semantic segmentation.

LabelMe, a labeling and annotation tool, was used for annotation [13].

Figure 15(a) shows shime-saba fillets manually annotated using LabelMe (red areas). Since the boundary is not clear in the area of fillet touching the conveyor belt, the darker area toward the fillet was treated as the boundary. To evaluate the derived model of semantic segmentation, we merged two fillet images horizontally and inferred the boundaries of each with the model. As shown in Figure 15(b), the two fillets can be separated, and the boundaries of each fillet (yellow lines) extracted are acceptable. The result is expected to enable the identification of the thickest part of the shime-saba fillet, which will facilitate the identification of areas of the pinbone tips.

VI. Conclusion

In this study, an image sensing system for detecting the pinbone tips of shime-saba was developed. The two-step processes of selecting local convex-up areas by mathematical quadratic surfaces and determining pinbone-containing areas by the Convolution Neural Network enable pinbone locations to be automatically identified. Pinbone detection accuracy was 84.9%, while Precision, Recall, and F-Measures were relatively low at just over 60%. As a first attempt, this result is acceptable. Further improvement in results can be expected by increasing the number of samples in the data set.

Since the area where pinbones are located is known to be in and around the middle of the fillet, the proposed cubic curve based on the edge information indicates that these areas can

be estimated. For a better method of obtaining the area, we found that automatic extraction of the fillet shape by semantic segmentation can also be used. This method enables simultaneous detection of pinbone tips from multiple fillets.

Future experiments will include the implementation of a deboning robot that will remove the detected pinbone tips. The results will be presented in our forthcoming paper.

ACKNOWLEDGMENT

This work was supported by the IoT Human Resource Development Support Project of Iwate Prefecture, Japan.

REFERENCES

[1] H. Ito, O. D. A. Prima, and T. Sasaki, "Detection of Pinbones in Japanese Shime-saba," The Fifteenth International Conference on Advances in Computer-Human Interactions, ACHI 2022, pp. 22-25, 2022.

[2] C. Alejandro, "Food Analysis: Present, Future, and Foodomics," International Scholarly Research Network (ISRN) Analytical Chemistry, pp. 1-16, 2012.

[3] P . Graham, "Robotic Equipment in the Meat Industry," Meat Science, 49(1), pp. 297-307, 1998.

[4] H. Einarsdottir, B. Guoundsson, and V. Omarsson, "Automation in the fish industry," Animal Frontiers, 12(2), pp. 32–39, 2022.

[5] D. Mery, et al., "Automated fish bone detection using X-ray imaging," Journal of Food Engineering, 105(3), pp. 485–492, 2011, https://doi.org/10.1016/j.jfoodeng.2011.03.007.

[6] V. Andriiashen, R. van Liere, T. van Leeuwen, K. J. Batenburg, "Unsupervised Foreign Object Detection Based on Dual-Energy Absorptiometry in the Food Industry," Journal of Imaging, 7(104), pp. 1-18, 2021.

[7] S. Wang, R. Nian, L. Cao, J. Sui, and H. Lin, "Detection of fish bones in cod fillets by UV illumination," Journal of Food Protection, 78(7), pp. 1414–1419, 2015. https://doi.org/10.4315/0362-028X.JFP-14-358.

[8] W. Wei, et al., "Enhanced chemical and spatial recognition of fish bones in surimi by Tri-step infrared spectroscopy and infrared microspectroscopic imaging," Spectrochimica Acta Part A: Molecular and Biomolecular Spectroscopy, 205, pp. 186–192. doi:10.1016/j.saa.2018.07.031, 2018.

[9] S. Song, et al., "Detection of fish bones in fillets by Raman hyperspectral imaging technology," Journal of Food Engineering, 272, pp. 1-10, 2019. https://doi.org/10.1016/j.jfoodeng.2019.109808

[10] B. G. Osborne, "Near-Infrared Spectroscopy in Food Analysis," Encyclopedia of Analytical Chemistry, pp. 1–14, 2006. https://doi.org/10.1002/9780470027318.a1018

[11] D. Wang, S. W. Laffan, Y. Liu, and L. Wu, "Morphometric characterisation of landform from DEMs," International Journal of Geographical Information Science, 24(2), pp. 305–326, 2010. https://doi.org/10.1080/13658810802467969.

[12] T. Narihira,et al., "Neural Network Libraries: A Deep Learning Framework Designed from Engineers' Perspectives," arXiv preprint arXiv:2102.06725, pp. 1- 12, 2021.

[13] LabelMe, https://github.com/wkentaro/labelme [retrieved: December, 2022].